Results from the BRAHMS experiment at RHIC

F.Videbæk [a]
BRAHMS Collaboration
I. G. Bearden[b], D. Beavis[a], C. Besliu[c], Y. Blyakhman[d], J. Brzychczyk[e], B. Budick[d], H. Bøggild[b], C. Chasman[a], C. H. Christensen[b], P. Christiansen[b], J. Cibor[f], R. Debbe[a], J. J. Gaardhøje[b], K. Grotowski[e], K. Hagel[g], O. Hansen[b], A. Holm[b], A. K. Holme[h], H. Ito[i], E. Jakobsen[b], A. Jipa, J. I. Jørdre[j], F. Jundt[k], C. E. Jørgensen[b], E. J. Kim[l], T. Kozik[e], T. Keutgen[g], T. M. Larsen[h], J. H. Lee[a], Y. K. Lee[l], G. Løvhøiden[h], Z. Majka[e], A. Makeev[g], B. McBreen[a], M. Murray[g], J. Natowitz[g], B. S. Nielsen[b], K. Olchanski[a], J. Olness[a], D. Ouerdane[b], R. Płaneta[e], F. Rami[k], D. Roehrich[j], B. H. Samset[h], S. J. Sanders[i], R. A. Sheetz[a], Z. Sosin[e], P. Staszel[b], T. F. Thorsteinsen[j+], T. S. Tveter[h], F. Videbæk[a], R. Wada[g], A. Wieloch[e], and I. S. Zgura

[a]Brookhaven National Laboratory, Upton, USA

[b]Niels Bohr Institute, University of Copenhagen, Denmark

[c]University of Bucharest, Romania

[d]New York University, New York, USA

[e]Jagiellonian University, Krakow, Poland

[f]Institute of Nuclear Physics, Krakow, Poland

[g]Texas A&M University, College Station, USA

[h]Fysisk Institutt, University of Oslo, Oslo, Norway

[i]University of Kansas, USA

[j]University of Bergen, Norway

[k]Institut de Recherches Subatomiques and Université Louis Pasteur,Strasbourg, France

[l]Johns Hopkins University, Baltimore, USA

The BRAHMS experiment at RHIC had its first data taking in August of 2000. From this first short run we have preliminary measurements of charge particle multiplicity distribution $dN/d\eta$ for central Au–Au collisions, spectra of charged hadron and ratios for identified particle at several rapidities. The anti-proton to proton ratios are compared to current models.

1. INTRODUCTION

The Broad RAnge Hadron Magnetic Spectrometers (BRAHMS) experiment is designed to gather basic information in heavy ion reactions on momentum spectra and yields for various emitted particles as function of transverse momenta, p_t, and rapidity, y. These yields as function of rapidity are important indicators of the densities reached in the collisions and of the produced entropy. The spectral shapes and their y-dependence reveal the reaction dynamics and the degree of thermalisation attained. The high p_t parts of the spectra carry information from the early times in the reaction. Global measurements of paritcle production, a measure of centrality, are an integral part of the experiment, and systematic studies are needed to establish an understanding of the reaction dynamics. The measurements in the short run of Au–Au collisions at $\sqrt{s_{NN}} = 130$ GeV at RHIC in 2000 focused on global observables and on first measurements of hadronic spectra, in particular particle ratios at mid and forward rapidities. These measurements,which are described below, shed light on the issue of stopping, chemical equilibration, and whether the mid-rapidity region is baryon free [1–3].

1.1. EXPERIMENTAL SETUP

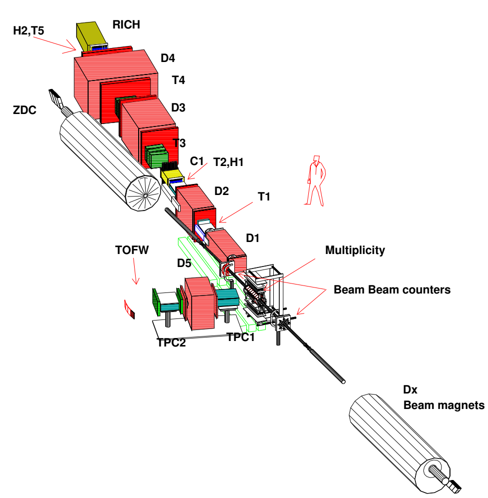

Figure 1. Schematic picture of the Brahms detector. Details of the setup are described in the text.

The BRAHMS experiment will measure well identified charged hadrons ($\pi^{\pm}, K^{\pm}, p^{\pm}$) over a wide range of rapidity and transverse momenta at all energies and beams available at RHIC. The very different experimental conditions, momenta, and particle densities at mid-rapidity and forward angles has led to a design with two moveable magnetic spectrometers.

The following is a brief description of the setup. More details can be found in [4]. The Mid-Rapidity Spectrometer (MRS) covers the angular region $30^\circ \le \Theta \le 95^\circ$ ($-0.1 \le \eta \le 1.3$) and the forward spectrometer (FS) the region $2.3^\circ \le \Theta \le 30^\circ$ ($1.3 \le \eta \le 4.0$). The solid angles subtended by the MRS and FS are 6.0 msr and 0.5 msr respectively. The FS consists of 4 dipole magnets (D1-D4), two time projection chambers (T1,T2), and three drift chamber modules (T3-T5). The particle identification is done by combining time-of-flight measurements in the hodoscopes H1 and H2 with data from the threshold Cherenkov counter C1 and the Ring Imaging Cherenkov Counter (RICH). The H1 and H2 consists of 48 and 32 scintillator, respectively. Each slats is read out from PMTs at top and bottom. This allows for particle identification in the momentum range 1-20 GeV/c in the forward spectrometer. The mid-rapidity spectrometer has two TPCs (TPC1 and TPC2), a dipole magnet (D5) for momentum measurements, and a time-of-flight wall (TOFW) at 4.3 m instrumented with 83 slats each 1.2 cm wide.

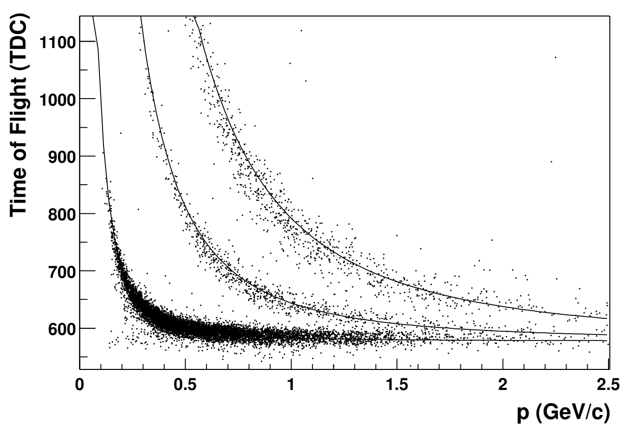

Figure 2. Time-of-flight performance for MRS at 90 deg. The lines shown are the predicted relationship between momentum and time-of-flight for pion, kaons, and protons, respectively.

Three event characterization detector systems provide global information, namely the Beam-Beam counters, a multiplicity detector, and a Zero-Degree calorimeter. The Beam-Beam counters provides the initial trigger and vertex information as well as the start time for the time-of-flight measurements. Each of the elements of the Beam-Beam counters consists of 3 and 4cm UVT Cherenkov radiators read out by PMTs. There is a total of 36 and 44 elements in the right and left counter positioned at ± 2.2 m, respectively. A multiplicity detector characterizes the centrality of the collisions in the mid-rapidity region. It is a hybrid detector consisting of 24 segmented Si-detectors for a total of 168 channels (SiMA), and 40 scintilator tiles (12*12cm)(TMA) covering the pseudo-rapidity range of $-2.0 \le \eta \le 2.0$. Zero-Degree Calorimeters (ZDC) [6], that are common devices for all RHIC experiments, are situated behind the two DX beamline magnets. They are used to measure the luminosity in Au–Au collisions, and to measure centrality by measuring forward going spectator neutrons. Together the three systems provide centrality coverage in the mid-rapidity region $-2.0 \leq \eta \leq 2.0$, in the region $3.2 \leq |\eta| \leq 4.3$ and at zero degree.

During the 2000 run the spectrometer measurements reported were taken with the MRS operated at 90°, 60°, and 40°, and the FFS consiting of the two TPCs T1,T2 and the time-of-flight wall H2, at an angle of 4°. The magnets were run at modest fields allowing the reconstruction of particle tracks with momenta above ≈ 0.2 GeV/c in the MRS and above ≈ 2 GeV/c in the FS. The BB counters have an intrinsic time resolution of 65 ps and permit a determination of the position of the collision vertex to a precision of ≈ 2 cm by measuring the difference in arrival time of the first particles in the left and right arrays assuming that these particles travel with the velocity of light. This method is confirmed by determining the vertex by projecting tracks determined in the first TPC of the MRS back to the beam plane.

The two TOF arrays are positioned at 4.3 m (MRS) and 8.6 m (FS) from the nominal interaction vertex position, respectively. No slewing corrections have been applied in the present analysis. The overall time resolution was determined to σ(TOF)$\approx$ 120 ps and thus permitted the separation of kaons and protons in the momentum range $p < 2.2$ GeV/c and $p < 4.5$ GeV/c in the MRS and FS, respectively. The excellent PID achieved is demonstrated in Fig. 2.

2. PERIPHERAL COLLISIONS

In addition to providing the experiments with luminosity information (see e.g. contribution [7] in these proceedings) the ZDCs can be used to probe very peripheral interactions of heavy ions. The ions produce intense electromagnetic fields which may be used to probe the structure of the nucleus. At $\sqrt{s_{NN}} = 130$ GeV one nucleus sees the other approaching at a speed corresponding to a Lorenz factor of $\gamma = 9800$. The nucleus may absorb several photons and be excited into the giant dipole or even to multi-phonon resonances. As the nucleus equilibrates and cools it may emit several neutrons, protons, and photons.

In order to study electromagnetic interactions it was required that no hits were recorded in either the tiles or the beam-beam counters. From simulations with the HIJING[8] event generator we estimate that there is an $\approx 2\%$ contamination of peripheral nuclear events in the sample. Figure 3 shows the energy spectrum in the right ZDC. The spectrum shows a strong one neutron peak, a smaller two neutron peak and then a continuum. Figure 3 also shows the energy spectrum from the RELDIS[9] model after smearing with the experimental resolution. RELDIS extends the Weizsacker-Williams method to mutual Coloumb dissociation. Photo-neutron cross sections measured in different experiments are used as input for the calculations of dissociation cross sections. The excited nuclei reach thermal equilibrium and then decay according to the statistical evaporation-fission-multi-fragmentation model [10].

The energy spread of the neutrons that hit the ZDCs their is set by their internal motion in the nucleus and is negligible compared to the energy resolution of the ZDC which is $\sigma_E = 14 GeV$ for one $65 GeV$ neutron. Therefore we can fit the spectrum to a series of Gaussian peaks at $n \cdot 65 GeV$ with width $\sqrt{n} \cdot \sigma_E$ and extract the multiplicity of 1, 2, 3

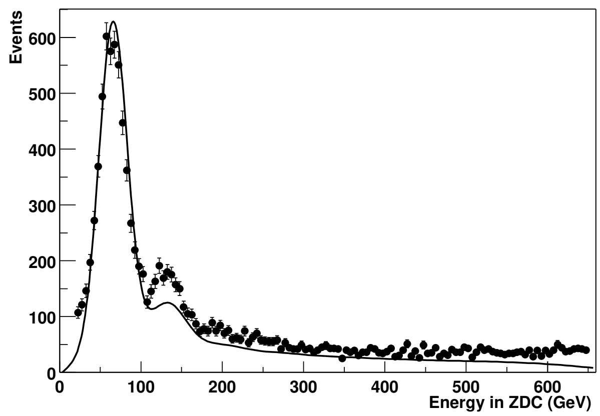

Figure 3. (a) The Zero Degree Calorimeter spectrum for electromagnetic events. The smooth curve shows the prediction of the RELDIS model normalized to the 1n yield.

etc neutrons. From the data we have extracted the ratio of yield of 2n to 1n emission to be 0.34 ± 0.03 a value that is higher than data extracted at lower energies[11] of ≈ 0.25. The probability to emit 2 neutrons rises with $\sqrt{s_{NN}}$, because more energy is absorbed and the multi-phonon resonances are more likely to be excited.

3. GLOBAL MEASUREMENTS

The global detectors were used for two measurements in the 2000 run, namely, a measurement of the overall charge particle production, and determining the collisions centrality. The TMA and SiMA are for most events hit by many particles including backgrounds. To transform this to a multiplicity measurement we rely on transforming the measured energy deposited into a number of hits. For each event and vertex position (and corresponding pseudo-rapidity), the total energy deposited in each element of TMA tiles or SiMA strip is accumulated. The energy loss signal is transformed to charged particle multiplicity via division with the expected average energy deposited by one charged primary particle in a tile. The expected energy, i.e. conversion factors, are evaluated by extensive GEANT simulations. Background particles contribute significantly to the deposited energy with about 10% for the SiMA and 30% for the TMA elements. The energy calibration of the detector elements comes from very peripheral event, pulser, cosmic ray, and source measurements. The solid angle and η is evaluated for each element from the actual vertex for each event and the contribution to the $dN/d\eta$ calculated. Centrality cuts are applied by selecting appropriate ranges in the multiplicity spectrum. The cuts can be expressed in terms of the fraction of the nuclear reaction cross section by normalization to the integral of the multiplicity spectrum obtained with a near minimum bias trigger. This trigger requires energy deposition in each of the two ZDCs above 25 GeV with the additional condition of at least one tile having a hit. This requirement selects events corresponding to $\approx 97\% \pm 2\%$ of the nuclear interaction cross section. The preliminary

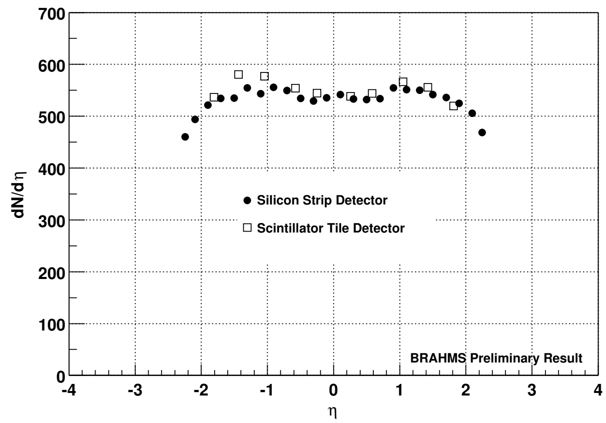

Figure 4. $dN/d\eta$ of charge particle as determined by TMA and SiMa detector systems for the most central 6% of the collisions.

$dN/d\eta$ distribution for the TMA and SiMA detector seperately is displayed in Fig.4 for a $0-6\%$ centrality cut. The distributions covering $-2.2 < \eta < 2$ agree well in both magnitude and shape. The small asymmetry present around $\eta = 0$ is believed to arise from the incomplete knowledge of the vertex position and contribute to the systematic error for $dN/d\eta$. The largest systematic error though is from the energy calibration of the detectors, and at the present stage of analysis the quoted systematic error is 10%. The value at $\eta = 0$ is found to be $dN/d\eta$= 530 $\pm$ 5(*statistical*) $\pm$ 50(*systematic*) and the distribution extends with about this value out to $\eta = \pm 2$ demonstrating a rather wide plateau for particle production. The front TPC of the mid-rapidity spectrometer also provide a measure of charge particle density. In addition to tracks that originate from the primary collisions, background tracks are also recorded. For each track we record the horizontal and vertical deviation of the tracks projected to the beam from the nominal vertex. The distributions are peaked at a small deviations, but has in addition a rather flat tail. The yield of primary tracks was extracted by a simultaneous fit to these distributions, normalized by the number of events in the 0-6% centrality class and the solid angles of the fiducial TPC volume. The preliminary result for the most central 0-6 of 550 $\pm$ 5 $\pm$ 50 is a good confirmation of the results for the global detectors. In addition these values for a centrality cut of $0-6\%$ is in good agreement with the published value from PHOBOS [12].

For the spectrometer analysis presented below three centrality bins using these detectors were used in the analysis (0 to 10%, from 10 to 20% and from 20 to 40% of the nuclear interaction cross section).

4. PARTICLE SPECTRA AND RATIOS

The key measurements for the BRAHMS experiment are those of charged hadrons. The spectra of negatively and positively charged hadrons h^+ and h^- has been determined near

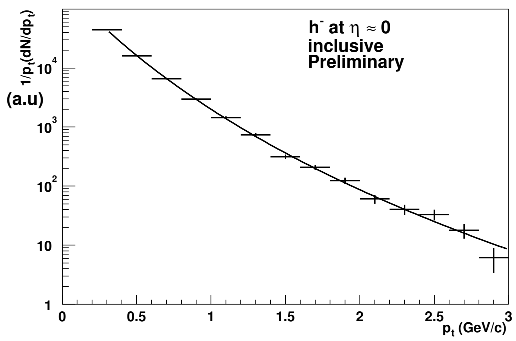

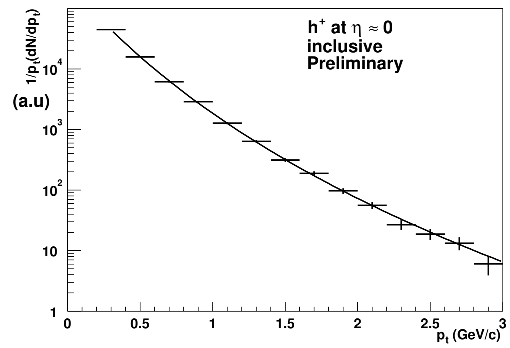

Figure 5. Invariant spectra of h- and h+ for $\eta \approx 0$ recorded with an inclusive trigger. The solid lines are power law fits as described in the text.

$\eta \approx 0$. The yield was corrected by using vertex dependent acceptance maps, with vertex position from -15 cm to + 15 cm, in a p_t range of 0.3 to 3 GeV/c. The accepted pseudo-rapidity range is $\Delta\eta = 0.1$. Figure 5 shows the arbitrary normalized yields $d^2N/d\eta dp_t^2$ for h^+ and h^-. They have similar shapes and both exhibit a typical power law dependence. The event selection corresponds to an average centrality cut of 18%. The $< p_t >$ has been determined by fitting the power law dependence, $A(p_t + p_0)^{-n}$, and found to be .480 and .450 GeV/c for positive and negative hadrons, respectively. This is somewhat higher than the value found by extrapolation results from ISR and UA1 of $< p_t >= .365$ GeV/c.

In the MRS, kaons and pions could be separated up to $p = 1.5$ GeV/c and protons from kaons up to 2.4 GeV/c. In the FS, kaons could not be cleanly separated from pions, although the $N(\pi^-)/N(\pi^+)$ ratio in the range $0.15 < p_t < 0.3$ GeV/c could be determined with only a small kaon contamination. Protons are seperated from kaons up to momenta of 4.5 GeV/c.

The number of particles measured at either polarity is normalized to the same number of collision events defined by the BB–ZDC coincidences fulfilling a given centrality cut described above and the ratios calculated. The acceptances for the spectrometers for positively charged particles at one field are equal to the acceptances for negatively charge particles at the opposite polarity. Thus in ratios of numbers of particles, measured at opposite field polarities most systematic errors cancel out in particular geometry and tracking efficiencies. The main source of systematic uncertainties in the particle ratios quoted stem from the run luminosity normalizations, from background slow background protons, and from corrections to anti-proton absorption. The normalizations contribute less than $\pm 5\%$. The data has not been corrected for contributions from weak decays of hyperon, but this is a small effect; less than 10% for a wide range of assumptions of hyperon yields and ratios.

The lower panel of Fig. 6 shows the dependence of the measured $N(\bar{p})/N(p)$ ratios on particle transverse momentum at mid-rapidity. Detailed information on the p_t and centrality dependence is given in [5]. Ratios were corrected for antiproton absorption,

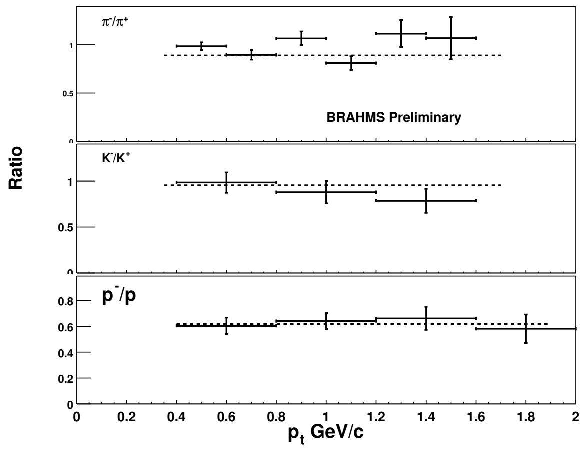

Figure 6. Particle ratios for pion, kaons and protons at $\eta \approx 0.$ in the centrality bin $0 - 40\%$.

and for contamination of background protons that is only of importance at the lowest momentum bin and is a 10% correction. The vertical error bars represent statistical errors only, while the horizontal bars indicate the bin size. The ratios exhibit very little centrality and p_t dependence. The value of $N(\bar{p})/N(p) = 0.62\ \pm 0.04\ \pm 0.05$ is obtained from integration over p_t in the centrality bin 0-40%. The is much larger than the heavy ion data at lower energies [13,14], but is comparable to extrapolations of pp data from the ISR[16] to $\sqrt{s_{NN}} = 130$ GeV. Our value is in good agreement with that presented by STAR [15].

The $N(\pi^-)/N(\pi^+)$ ratios displayed in the top panel exhibit a similar lack of centrality and p_t dependence. The average value of $N(\pi^-)/N(\pi^+) = 0.95 \pm 0.03 \pm 0.05$ demonstrates the high degree of isospin equilibration in the reaction. In addition this ratio is consistent with unity for the 3 rapidity points measured by BRAHMS up to $y \approx 0$. The $N(K^-)/N(K^+)$ ratios displayed in the top panel also exhibit no centrality and p_t dependence. The value of $N(K^-)/N(K^+) = 0.89 \pm 0.07 \pm 0.05$ is considerable higher than at AGS, and SPS energies and shows that the expected equilibration has almost been reached at $\sqrt{s_{NN}} = 130$GeV.

Particular interest is attached to the rapidity dependence of the $N(\bar{p})/N(p)$ ratio shown in Fig.7. The present systematics show that the ratios fall off more rapidly over two units of rapidity than the nucleus-nucleus results at lower $\sqrt{s_{NN}}$, but are very similar to the p+p result at roughly half the CM energy [17].

Also in Fig. 7 we compare the measured ratios to calculations using the HIJING model [8], the FRITIOF 7.02 [18] string model and the UrQMD cascade model [19] using the same cuts on centrality as those applied in the data analysis. The FRITIOF model reproduces the $N(\bar{p})/N(p)$ ratios quite well, while it overpredicts by $\approx 30\%$ the charged particle yield at $\eta \approx 0$ [12]. This is mainly related to a fairly large degree of stopping predicted by the model. On the other hand the HIJING model descibes the overall charge particle yields at $\eta \approx 0$ while fails in describing the anti-proton to proton ratios rapidity

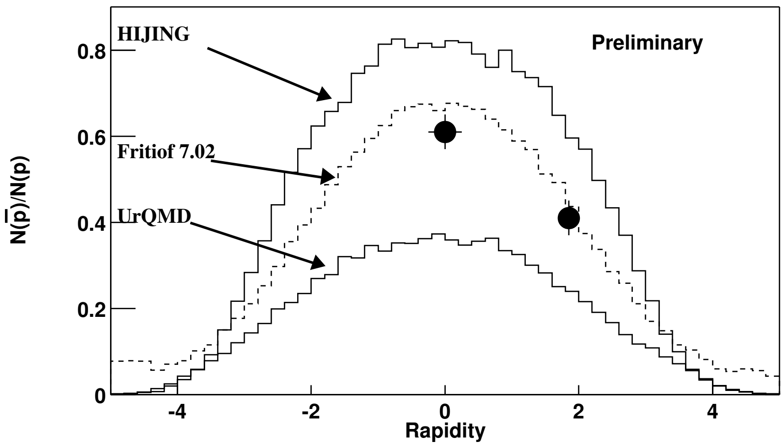

Figure 7. Rapidity dependence of the ratio $N(\bar{p})/N(p)$ and comparison to model predictions. The data shown are for $0-40\%$ central events and integrated over the transverse momentum range given in the text. The three calculations using the HIJING model, FRITIOF and UrQMD models discussed in the text are shown.

dependence. This feature of the model is in turn related to a small stopping of the projectile baryons. The UrQMD model, which is not a partonic model, underpredicts the ratios by almost a factor of 2. These models exemplify the present understanding of heavy ion collisions at this new energy regime; none of the models offers a consistent description of the observed features and the rapidity dependence serves as a benchmark for the description of stopping and anti-baryon production.

5. SUMMARY

The first preliminary data from the BRAHMS experiment at RHIC from Au–Au collisions at $\sqrt{s_{NN}}$=130 GeV has been reported. From 3 independent detectors we have obtained the pseudo-rapidity density for the most $0-6\%$ central Au–Au collisions $dN/d\eta$ of$\approx$ 530 with an systematic error of 10%. Particle ratios pions and kaons are close to unity at mid-rapidity. The ratio of antiprotons to protons is significantly below unity at mid-rapidity, and decrease at forward rapidity. The rapidity dependence serves as a strong indicator of the balance between stopping of projectile baryons and anti-baryon baryon production.

The BRAHMS collaboration wishes to thank the C-AD department of BNL for successful commissioning of RHIC and the contributions to the construction of the experiment. This work was supported by the Division of Nuclear Physics of the Office of Science of the U.S. Department of Energy under contract with BNL (No.DE-AC02-98CH10886), Texas A&M (DE-FG03-93ER40773), U.Kansas (DE-FG03-96ER40981), NYU (DE-FG02-99ER41121), the Danish Natural Science Research Council, the Korea Research Foundation Grant, the Norwegian Natural Science Research Council, the Jagiellonian University Grant, and the Romanian Ministry of Education and Research

REFERENCES

1. J.D. Bjorken, Phys. Rev. **D27**, 140 (1983).
2. N. Herrmann, J.P. Wessels and T. Wienold, Annu. Rev. Nucl. Part. Sci. **49**, 581 (1999).
3. F. Videbæk and O. Hansen, Phys. Rev. **C52**, 2584 (1995).
4. D. Beavis et al., The BRAHMS collaboration, 'Conceptual Design Report for BRAHMS', BNL-62018 (/www.rhic.bnl.gov/brahms/WWW/cdr/cdr.html).
   I.G. Bearden et al., The BRAHMS collaboration, Nuclear Instruments and Methods, to be published;
5. I.G.Bearden for the BRAHMS collaboration, these proceedings.
6. C.Adler et al., Nucl. Inst. Meth.(2001) submitted, (/xxx.lanl.gov/nucl-ex/0008005).
7. A.Denisov,*Common event characterization in the RHIC experiments.* These proceedings.
8. HIJING with Parton shadowing and Jet quench. X-N. Wang and M. Gyulassy, Phys. Rev. D **44** (1991) 3501.
9. I.A. Pshenichnov, J.P. Bondorf, I.N. Mishustin, A. Ventura, S. Masetti nucl-th/0101035; nucl-th/0007017; Phys. Rev. **C60** 044901 (1999) and nucl-th/9901061; Phys. Rev. **C57** 1920 (1998) and nucl-th/9711030; K.A.Chikin, V.L.Korotkih, A.P.Kryukov, L.I.Sarycheva, I.A.Pshenichnov, J.P.Bondorf, I.N.Mishustin, Eur.Phys.J. **A8** 537 (2000), I.A. Pshenichnov, nucl-th/9912008
10. J.P. Bondorf, A.S. Botvina, A.S. Iljinov, I.N. Mishustin and K. Sneppen, Phys. Rep. **257**, 133 (1995).
11. J. C. Hill, F. K. Wohn, J. A. Winger, M. Khayat, and K. Leininger,Phys Rev C **38** 1722 (1988); J. C. Hill, F. K. Wohn, J. A. Winger, M. Khayat, and M. T. Mercier,ibid **39** 524 (1989); T. Aumann, J. V. Kratz, and E. Stiel ibid. **47** 1728 (1993),J. Hill, HIPAGS 96 p 286 J. C. Hill, A. Petridis, B. Fadem, F. K. Wohn, Nucl. Phys. A**661** 313c (1999)
12. B.Back et.al. Phys.ReV.Lett.**85**,3100(2000).
13. L. Ahle et al., The E802 collaboration, Phys. Rev. Lett. **81**, 2650 (1998).
14. I. G. Bearden et al, NA44 collaboration, J. Phys. G, Nucl. Part **23** (1997) 1865, and *Particle production in Pb+Pb collisions at CERN-SPS* (in prep).
15. C. Adler et al., The STAR collaboration, Phys. Rev. Lett., (in print)
16. K.Guettler et al. Nucl.Phys.**B116**, 77 (1976)
17. P. Capiluppi et al., Nucl. Phys. **B79**, 189 (1974).
18. B. Andersson, G. Gustafson, H. Pi: Z. Phys. **C57**, 485 (1993) ; H. Pi, Comp. Phys. Comm. **71** 173(1992).
19. S. A. Bass et al, Prog. Part. Nucl. Phys. **141** (1998) 225 and M. Bleicher et al. J. Phys. G. Nucl. Part **25** 1859 (1999).